THERMAL ASSEMBLY OF POLYSILICON MICROACTUATORS WITH NARROW-GAP ELECTROSTATIC COMB DRIVE

G. K. Fedder, J. C. Chang, and R. T. Howe

University of California at Berkeley
Department of Electrical Engineering and Computer Sciences
and the Electronics Research Laboratory
Berkeley Sensor & Actuator Center
Berkeley, California 94720 USA

ABSTRACT

New surface micromachined, polysilicon fuse and weld microstructures are modeled, fabricated, and characterized. The current required to cut the thin, 2000 Å fuse is 30 mA, compared to 80 mA for a 2 μm-thick fuse. For large currents, a simple model shows that the time to cut a fuse is inversely proportional to the square of the current. An aluminum microbridge is used to form a robust weld, connecting two polysilicon structures. The surface tension of the molten Al produces a force of approximately 15 μN, which is about 100 times larger than electrostatic comb drive forces. A series of current pulses is used to melt the Al without destroying the weld joint. A two-dimensional temperature distribution, calculated using a custom finite element program, is helpful in design of the welding structure. One application incorporating both the fusing and welding process is a microactuator connected to a highly compliant suspension. The most aggressive design will move 11 μm with 10 V applied to a 1 μm-gap comb drive.

I. INTRODUCTION

Surface micromachining involves the selective etching of a sacrificial layer surrounding a patterned microstructural layer. After rinsing and drying, free-standing micromechanical elements are produced. For many microstructures, this basic process suffices for their *in situ* fabrication. However, microstructures with highly compliant suspensions are susceptible to breakage, or to attachment to the substrate, or attachment to each other, due to surface tension forces in the final rinse and drying step [1]. In addition, micromechanical systems with sub-micron spacing between elements are difficult to fabricate using conventional lithography and etching. For example, it is desireable to design sub-micron gaps between the stator and movable comb in a lateral resonator to increase the electrostatic force for a given applied voltage. Finally, run-to-run variations in the mechanical properties of thin films can alter the mechanical behavior of sensitive structures, such as resonators with clamped suspensions.

Thermal microassembly, an extension of surface micromachining, addresses these drawbacks [2]. The concept involves the post-release fusing and welding, under electrical control, of portions of the suspended microstructure. Direct manipulation of the structure is unnecessary and, therefore, the cost of adjustment or assembly of wafers at a wafer probe station is eliminated. An example application is the use of fuses to constrain a high-sensitivity accelerometer, protecting it against breakage or stiction during rinsing [3].

In this paper, we present improved versions of the resistively heated polysilicon fuse and the welding structure. The latter incorporates an Al film in order to provide an attractive force due to surface tension. The fuse uses a thin polysilicon film in order to reduce the cutting current. Test structures are used to test simple models for the two processes. In order to demonstrate the application of thermal microassembly, we describe a narrow-gap comb drive actuator with a highly compliant suspension. Both fuses and welds are used to assemble this structure, after release from the substrate.

II. FABRICATION

Mechanical microstructures, thin polysilicon fusible supports, and Al welding structures are integrated into a nine-mask process (Figure 1). The initial processing steps are similar to the first comb-drive resonator process [4]. After each processing step is discussed, the corresponding part of Figure 1 will be stated in parenthesis.

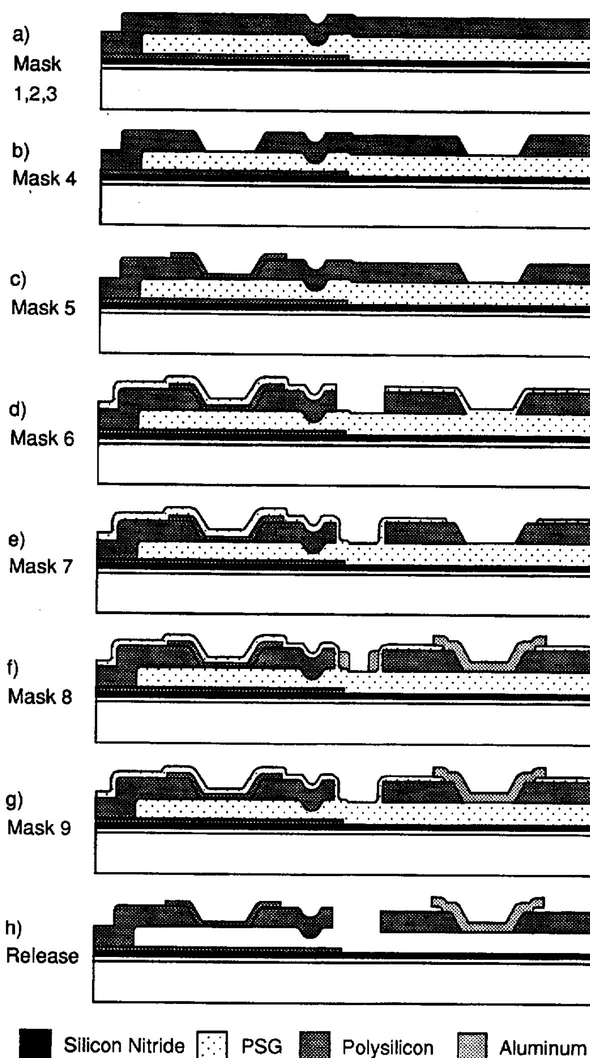

Figure 1: Cross-sections of the nine-mask process flow.

Silicon nitride is deposited over thermal silicon dioxide to electrically isolate structures from the silicon substrate. A 3000 Å *in situ* doped polysilicon film is deposited and plasma etched in CCl_4 to form an interconnect layer. Next, 2 μm of PSG is deposited as a sacrificial spacer for the polysilicon microstructures. Dimples are fabricated on the underside of the structural polysilicon by doing a timed wet etch of the sacrificial PSG. Contact cuts are made to the underlying polysilicon layer using a CHF_3/CF_4 plasma etch. An undoped, 2.5 μm-thick polysilicon structural layer is deposited at 605 °C, 250 sccm SiH_4, and 550 mTorr, producing a slightly tensile film [5] (a). An additional 0.5 μm of PSG is deposited and annealed for one-hour at 950 °C to dope the polysilicon and reduce stress gradients in the film. After stripping the top layer of PSG, trenches in the polysilicon structural layer are formed (b). Fusible supports and Al microbridges will be placed in these trenches. The photoresist mask is ashed in O_2 plasma for 7 minutes at 50 W to ensure sloped sidewalls. A CCl_4 plasma etch transfers the sidewall pattern to the polysilicon trench. Next, 2000 Å of *in situ* doped polysilicon is deposited directly on top of the structural polysilicon. A timed CCl_4 plasma etch defines the fusible supports in the trenches (c). Another 0.8 μm of PSG is deposited and densified using RTA at 1050 °C for 1 minute. The PSG is patterned and used as a mask for the structural polysilicon etch. Structural etching was deferred until after etching the fusible supports, so the thin polysilicon fuse layer does not conformally coat the structures and affect their mechanical integrity. Plasma etching combined with the PSG mask results in straight sidewalls on the mechanical microstructures (d). After an additional 3000 Å of PSG is deposited, the PSG is patterned and wet etched to form contact cuts for the subsequent Al layer (e). The sputtered 1.5 μm-thick Al, used in the welding structures, is etched in a Cl_2 plasma (f). A final mask is used to protect the Al weld joints during wet etch of Al sidewalls (g). A 1 minute concentrated (49%) HF etch releases the microstructures without noticeably attacking the Al (h) [6].

III. MODELING AND NUMERICAL ANALYSIS

A. Resistive Cutting

A one-dimensional model for resistive heating of polysilicon microbridges is described elsewhere [2, 7]. Since the fuse is short, convection and radiation components of heat flow can be neglected. Heat loss by conduction out the ends of the fuse and through the air to the substrate is approximately proportional to the temperature of the bridge. When a step of current is passed through the fuse, the temperature of the fuse rises with time constant, τ. If the resistance of the fuse is assumed to be constant, the net heat flow into the fuse, $\dot{Q}_{net}$, can be approximated as decreasing exponentially with time constant, τ.

$$\dot{Q}_{net} = \dot{Q}_g - \dot{Q}_l = I^2 R e^{-t/\tau} \quad (1)$$

where $\dot{Q}_g$ is the ohmic power generated, and $\dot{Q}_l$ is the heat loss. The energy required to cut a fuse, Q_c, is the integral of the net heat flow.

$$\int_0^{t_c} \dot{Q}_{net} dt = Q_c \quad (2)$$

Solving Equation (2) gives an expression for the time required to cut a fuse, t_c.

$$t_c = \tau \ln \left[\frac{1}{1 - \left(\frac{I_c}{I}\right)^2} \right] \quad (3)$$

where $I_c \triangleq \sqrt{Q_c/\tau/R}$ is the current required to cut a fuse. For $I < I_c$, the time to cut becomes infinite. When $I \gg I_c$, the conductive heat loss is negligible compared to the heat generation, and $t_c \propto I^{-2}$. For currents close to I_c, the heat loss is significant, and it takes longer to cut the fuse.

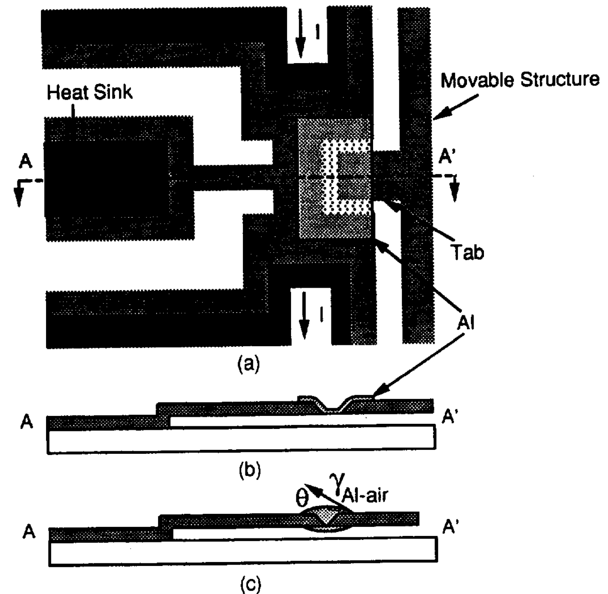

Figure 2: Schematic drawing of a welding structure. a) Top view. b) Side view. c) Side view after melting Al.

B. Resistive Welding

Past attempts at welding polysilicon structures have not been very successful [2]. Current was passed through the mechanical joint, where it is difficult to make reliable electrical contact, because of native oxide. The second-generation welding structure is shown in Figure 2. The current path is symmetric, beginning at one anchored pad, through a 8 μm-wide by 12 μm-long polysilicon filament, to another anchored pad. A 4 μm-wide anchored beam is connected to the center of one side of the filament, to reduce the temperature of the side opposite the movable microstructure. A tab on the movable microstructure is connected to the polysilicon filament by an Al microbridge. When sufficient current is applied, the heated filament melts the Al and a permanent weld joint is formed. Related work has involved formation of aluminum filaments in polysilicon bridges by diffusion of metal from contact pads [8]. Si and Al mix to form an eutectic with a minimum melting point of 577 °C.

A schematic cross-section of the welded joint is shown in Figure 2(c). Surface tension of the molten Al provides a lateral force which is strong enough to pull the movable microstructure into contact with the polysilicon filament. The lateral force has components due to surface tension, F_{st}, and Laplace pressure, F_p [9]. Assuming that the molten Al surrounds the movable tab, the lateral component of surface tension is integrated around the beam to obtain the first force component.

$$F_{st} = 2(w + z_o)\gamma_{Al-air} \cos(\theta) \quad (4)$$

where w and z_o are the width and thickness of the movable tab, γ_{Al-air} is the surface tension of Al in air, and θ is the contact angle.

The Laplace pressure difference between the molten Al and air contributes a second component of force. The pressure difference is found by equating the work done by expansion of the molten liquid to the increase in total surface energy.

$$F_p = w z_o \frac{\gamma_{Al}}{R} \quad (5)$$

where γ_{Al} is the surface tension of Al in vacuum, and R is the radius of curvature of the molten Al.

An experimental value for surface tension of Al in argon, and in vacuum, has been found to be 0.865 N/m [10]. This value is assumed to be valid in air. The measured contact angle of different welding

structures varies between 0° to 45°. The movable tab connected to the Al is 8 μm wide and 2 μm thick. When the weld gap is zero, as shown in Figure 2(c), the measured radius of curvature is greater than 12 μm. Adding Equations (4) and (5) gives a value between 11 and 17 μN for lateral force. The Laplace pressure accounts for about 10% of the total calculated force. For comparison, a comb drive with twenty 2 μm-thick fingers, a 2 μm gap, and 20 V applied to the fingers generates 88 nN. The welding structure provides a force which is 100 times larger.

The temperature distribution of the welding structure can be approximated as two-dimensional, with no variation in the vertical dimension. The structural polysilicon has thickness, z_o, and is raised above the substrate surface by a distance, s. The two-dimensional heat equation is found by equating the heat conduction out of a differential element to the ohmic power generated in the element.

$$\nabla \cdot \kappa \nabla u - \frac{\kappa_a}{s\, z_o}(u - T_s) = -\,|\mathbf{J}|^2 \rho \qquad (6)$$

where $u(x, y)$ is the temperature of the bridge, $\mathbf{J}$ is the current density, ρ is the electrical resistivity of the bridge, κ_p is the thermal conductivity of the microstructure, κ_a is the thermal conductivity of air, and T_s is the substrate temperature.

Since the anchor pads are not perfect conductors of heat, the temperature at the anchored end of the structure will not be constant. Heat conducted through the pad can be modeled by a linear relationship, $\alpha(u - T_s)$, where α is the effective thermal conductance of the pad (with units of W/°K). Heat flow out the free sides and top of the plate is neglected.

The current density can be found from charge continuity and the constitutive relationship, $\mathbf{J} = \sigma \mathbf{E}$.

$$\nabla \cdot \mathbf{J} = \nabla \cdot \sigma \mathbf{E} = -\nabla \cdot \sigma \nabla \Phi = 0 \qquad (7)$$

$$\mathbf{J} = -\sigma \nabla \Phi \qquad (8)$$

where $\sigma = 1/\rho$ is the electrical conductivity, $\mathbf{E} = -\nabla \Phi$ is the electric field and Φ is the electrostatic potential.

Equations (6) and (7) are coupled through the temperature dependence of the resistivity. At temperatures below 1100 °C, the resistivity of heavily doped n-type polysilicon increases linearly with temperature [7]. To simplify the present analysis of welding structures, a constant resistivity is assumed. Constant thermal conductivities of polysilicon and the ambient are also assumed.

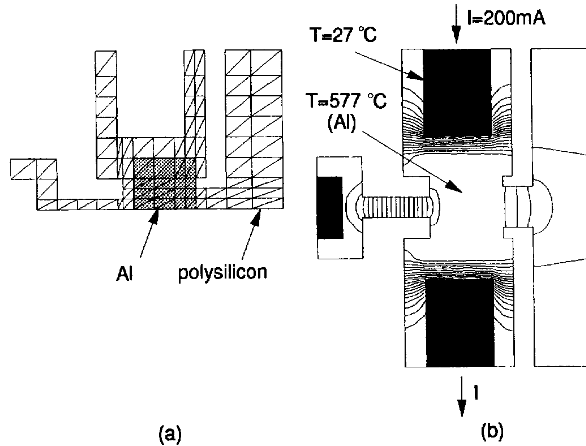

Figure 3: Two-dimensional finite element analysis of welding structure. a) Discretization into 146 quadratic triangular elements. b) Temperature distribution. Isotherms are spaced 27.4 °C apart.

The finite element method is used to solve Equations (6) and (7), including general natural boundary conditions to model the thermal conductance of the anchor pad. The welding structure, discussed earlier, is divided into 146 quadratic triangular elements as shown in Figure 3(a). Only half of the structure is modeled, exploiting symmetry. The movable plate is placed in complete contact with the cantilever support. Two × two point Gaussian integration is used to calculate element entries.

Values for the model parameters have been determined experimentally:

z_o=2 μm

s=2.5 μm

κ(polysilicon) = 32 W/m/°K [12]

κ(Al) = 237 W/m/°K [10]

κ_a = 0.051 W/m/°K at 400 °C [10]

$\rho = 3.7\times10^{-5}$ Ω−m

T_s = 27 °C

Figure 3(b) shows the thermal distribution of the welding structure for an applied current of 200 mA. For this case, the temperature of the Al is 577 °C. The finite element analysis does not model the polysilicon under the Al. Although a three-dimensional analysis would be more appropriate, the two-dimensional analysis does help in designing the welding structures.

IV. EXPERIMENTAL RESULTS

A. Resistive Cutting

Current, voltage, and energy values used in the cutting process are experimentally characterized. In one experiment, a capacitor is charged to 10 V, nominally, and then discharged through a fuse. The energy required to cut the fuse is determined by measuring the capacitor voltage before and after cutting. For a 2 μm-wide, 10 μm-long, and 1700 Å-thick fuse, with a sheet resistance of 40 Ω/□, 150±10 nJ is dissipated, independent of the capacitance value. This energy level is significantly higher than that needed to raise the volume of polysilicon to the melting point, 11 nJ. There is a large contact resistance between the metal micromanipulator probe tips and the polysilicon pads. After measuring the contact resistance, the actual energy generated in the fuse is estimated to be around 38 nJ. Resistive cutting of the fuses requires energy levels higher than that needed to melt the fuse.

Current pulses can also be used to cut fuses. A clean cut for the 1700 Å-thick fuse takes place in less than 1 μs, and requires at least

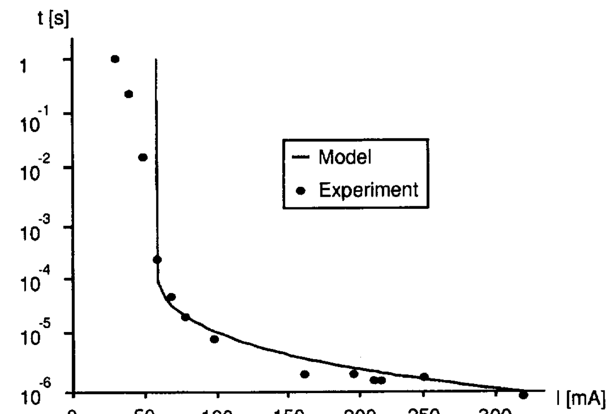

Figure 4: Time required to cut a 2 μm-wide, 10 μm-long, 2 μm-thick polysilicon fuse as a function of applied dc current.

30 mA. An identical fuse, but 2 μm-thick and 33 $\Omega/\square$, is cut cleanly with 80 mA in 19 μs. The cutting current does not appear to scale linearly with thickness. However, the reduced current level allows the fuses to be successfully connected in parallel, without destroying contacts. Interconnect resistance has limited successful cutting to four fuses in parallel. In larger arrays, not all of the fuses cut cleanly, since different values of current are passing through each fuse.

The current pulse generator used in the measurements is limited in bandwidth to 1 MHz, so the current is not constant for cutting time less than several microseconds. Thick polysilicon fuses take longer to cut, so accurate cutting time versus current measurements can be made using a digitizing oscilloscope. A plot of cutting time versus applied dc current for the thick fuses is given in Figure 4. Equation (3) is fit to the measured data using $I_c = 60$ mA and $\tau = 28\mu$s. For large currents, the power generated in the fuse is much greater than the heat conduction out of the fuse. If the heat loss is neglected, the time to cut should vary as $1/I^2$, assuming constant energy to cut a fuse. For small currents, the heat loss is significant, and it takes longer to cut the fuse. The fuse melts at currents between 20 and 60 mA and eventually open-circuits due to surface tension of the molten polysilicon.

Practical fusible supports must be designed as a loop to avoid passing current through the microstructure. Polysilicon fuses, 2 μm-wide, 12 μm-long, and 2000 Å-thick, are shown before and after resistive cutting in Figure 5. A current pulse of 140 mA is used to cut each fuse. Polysilicon residue, left on the substrate after cutting, is a result of cylindrical instability of the molten filament during cutting [9]. Thick fuses do not leave a residue, since the surface tension wicks all of the molten polysilicon to the two anchored ends. Further development of the cutting procedure may eliminate the residue left by the thinner fuses. By partly melting the thin fuses before cutting, all the material may wick to the ends.

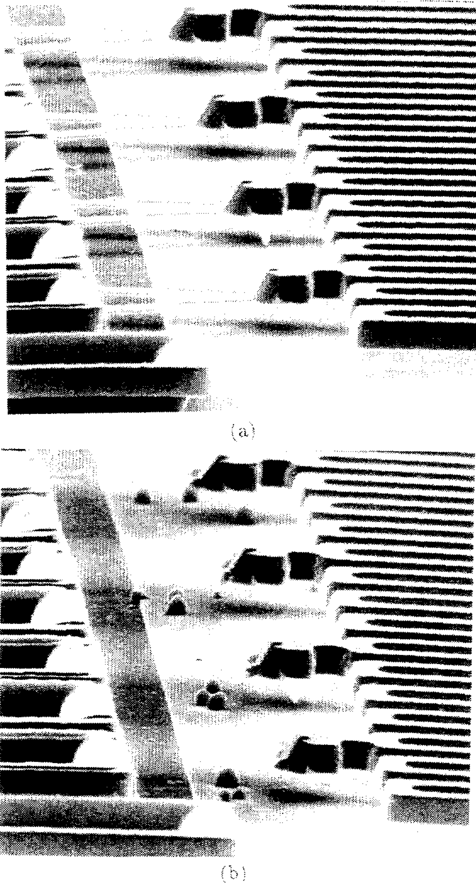

Figure 5: Scanning electron micrograph of 2 μm-wide, 10 μm-long, 2000 Å-thick polysilicon fuses supporting a serpentine spring. a) Before cutting. b) After cutting.

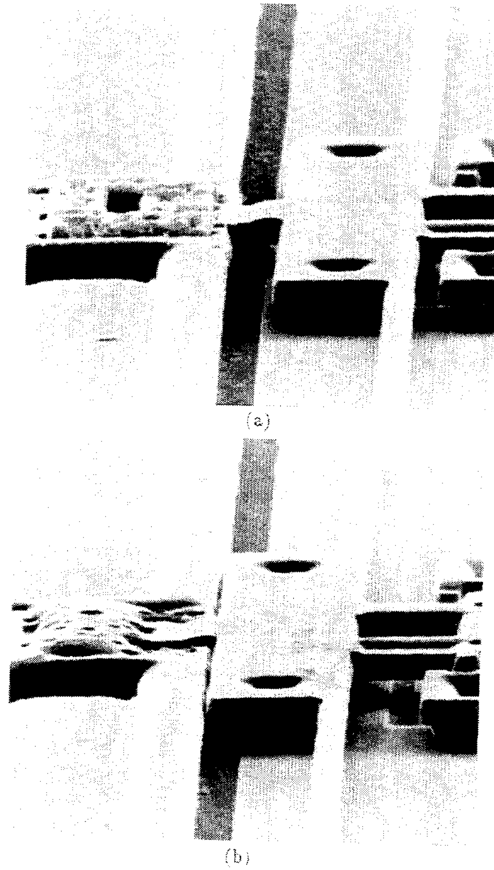

Figure 6: Scanning electron micrograph of a weld joint. a) Before welding. b) After welding.

Many of the fuses, such as those shown in Figure 5, are used to support very compliant serpentine springs. The fuses keep the structure from moving, and possibly breaking, during the sacrificial wet etch and rinse. If fuses are placed more than 300 μm apart, $2\mu\text{m} \times 2\mu\text{m}$ beams are stuck to the substrate.

B. Resistive Welding

A weld joint, before and application of current, is shown in Figure 6. The Al microbridge starts melting at an applied dc current of 100 mA. The finite element result is larger, probably because current spreading in the polysilicon underneath the Al is not modeled. Welding with dc current produces uncontrolled melting and migration of the Al, resulting in poor quality welds or destroyed structures. Instead, a robust welding procedure, using pulsed current, is arrived at empirically. For the most common welding structure, sixty, 5 μs wide, 50 % duty cycle, 500 mA current pulses are used to produce the best quality weld joints. Different welding structure layouts require separate characterization. The largest deflection observed is 6 μm.

A series of nine test structures are used to measure the lateral force, F, of the molten Al weld joint. One of the welding test structures is shown in Figure 7. Each structure is suspended by a folded flexure with a different spring constant, k_x. Measured lateral deflection, Δx, after each structure is welded into place, is given in Table 1.

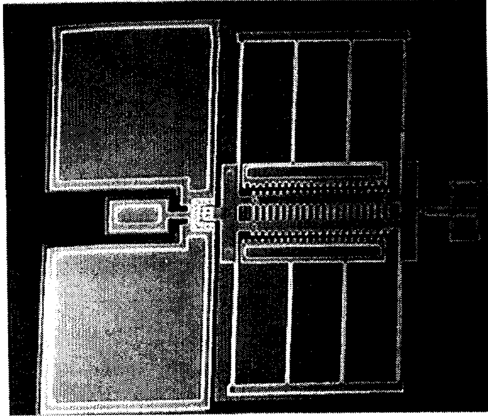

Figure 7: Scanning electron micrograph of welding structure used to measure lateral force.

Table 1: Measured deflection for lateral force test structures

#	k_x [N/m]	Δx [μm]	F [μN]	normalized F
1	0.27 ± 0.08	3.8 ± 0.1	0.95 ± 0.20	0.063 ± 0.002
2	0.53 ± 0.15	3.8 ± 0.1	1.9 ± 0.39	0.13 ± 0.004
3	1.3 ± 0.39	3.8 ± 0.1	4.8 ± 0.98	0.32 ± 0.095
4	2.7 ± 0.77	3.8 ± 0.1	9.5 ± 2.0	0.63 ± 0.019
5	5.3 ± 1.6	3.0 ± 0.1	15 ± 3.1	1
6	13 ± 3.9	1.6 ± 0.1	20 ± 4.2	1.3 ± 0.067
7	27 ± 7.7	1.0 ± 0.1	25 ± 5.4	1.7 ± 0.12
8	53 ± 15	0.6 ± 0.1	30 ± 7.1	2.0 ± 0.24
9	133 ± 39	0.4 ± 0.1	50 ± 14	3.3 ± 0.59

For k_x < 5.3 N/m, the movable structure hits a mechanical stop, which is designed to allow up to a 4 μm deflection. Measurement errors of beam width and thickness account for the error bounds for the spring constant values. Deflection is measured with a 0.2 μm vernier, giving error bounds of ± 0.1 μm. Values of normalized force have smaller error bounds, since the dimensional errors are not included.

Measured and calculated values of force agree for structure #5. The lateral force becomes larger for smaller deflections. As shown schematically in Figure 2(b), the Al microbridge starts out as a 1.5 μm film. As the movable structure deflects, the gap between the movable structure and the polysilicon anchor decreases. When the gap is large, there is not enough Al to completely fill the gap region. A negative radius of curvature of the Al in the gap would lower the Laplace pressure and increase the lateral force.

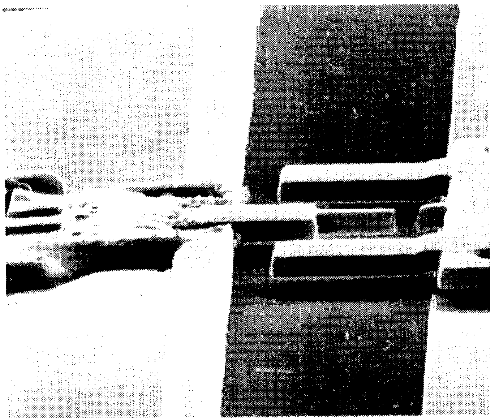

Figure 8: Scanning electron micrograph of structure used to measure weld strength, showing the fracture of a 2 μm × 2 μm beam and the intact weld joint.

Several structures, one of which is shown in Figure 8, have been fabricated to test weld joint strength. A micromanipulator probe tip provides the force to pull on the weld joint. The 2 μm × 2μm beam fractured at an estimated axial force of 6 mN, based on 1 % fracture strain for polysilicon [11]. The large puller cracked in half on structures with 2 μm × 4μm and 2 μm × 6μm beams. Forces at least 1000 times greater than typical electrostatic forces are required to fracture the weld joint.

C. Microactuator Design

Several microactuators, with different comb drives and suspensions have been designed and fabricated. A microactuator suspended by four very compliant serpentine springs is shown in Figure 9. Thin polysilicon fuses, which hold the springs in place during sacrificial etch, are cut to release the shuttle mass. Narrow-gap comb drives are located on both sides of the shuttle mass, Comb fingers are fabricated unengaged, so the wide gaps can be easily etched. Two welding structures are attached to each stator comb drive. The lateral force of the welding structures is used to engage the comb fingers. This assembly method is similar to the oxidation machining process [13], however, oxidation is not used to adjust the size of the comb finger gap. By moving the two sets of stator comb fingers, instead of moving the shuttle mass, a symmetric resonator drive is formed [14]. The welding structures provide strong, permanent connections. We have not been successful in engaging the stator comb drives, probably because the mechanical coupling of the two welding structures affects proper operation. When not mechanically coupled, welding structures of an identical design work reliably. Different welding processes for coupled welding structures will be explored. A modified layout, using only one welding structure on the stator, should produce a working microactuator.

The comb drives in Figure 9 have 20 fingers and a 1 μm gap. An electrostatic force of 44 nN, obtained from finite element analysis [15], is calculated for 10 V applied between the fingers. The serpentine springs are designed to have a spring constant of 1 nN/μm, obtained from finite element analysis using simple beam theory [16]. These springs allow the shuttle to move 11 μm with 10 V across the comb drive.

Thermal assembly of the microactuator consists of three steps: 1) cutting of fuses to release the folded flexure, which holds up the stator, 2) welding of the stator to engage the narrow-gap comb fingers and permanently anchor the stator, and 3) cutting of fuses to release the serpentine springs.

V. CONCLUSIONS

Thick polysilicon micromechanical structures, thin polysilicon fusible supports, and Al welding structures are combined in a nine-mask process. Around 35 nJ of energy is required to cut thin, 2000 Å

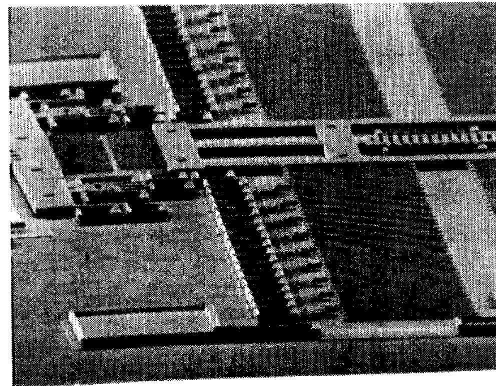

Figure 9: Partially assembled microactuator showing released serpentine springs and one of the unengaged comb drives (on the left).

fuses. A simple heat flow model predicts a I^{-2} dependence on the time needed to cut a fuse. The thin fuses are cut in less than 1 μs. Current required to cut the thin fuses (30 mA) is less than for 2 μm-thick fuses (80 mA), however, the reduction does not scale linearly with thickness. Long, thin fuses leave polysilicon residue on the substrate after being cut because of cylindrical instabilities in the molten fuse. We will explore different fuse designs and cutting procedures to obtain cuts with no residue.

A robust welding structure is made from an Al microbridge, which connects a polysilicon anchor with a movable polysilicon microstructure. A train of sixty, 5 μs, 500 mA current pulses produces a good weld joint. Lateral forces in excess of 15 μN are produced by surface tension of the molten Al. The completed weld joint can withstand forces greater than 6 mN without failure. Lateral deflections as large as 6 μm have been observed. A two-dimensional temperature distribution, calculated using a custom finite element program, aids in the welding structure design.

A microactuator, which incorporates both welding and fusing, has been designed and fabricated. Large serpentine springs provide a 4 nN/μm suspension. Thin polysilicon fuses, which support the springs, prevent damage and sticking to the substrate during the sacrificial PSG etch. Welding structures are used to move both sets of stator comb fingers. A three-step thermal assembly process creates a symmetric, 1 μm-gap comb drive microactuator. The most aggressive design is expected to move 11 μm with 10 V applied to the comb drive. Difficulties with the operation of mechanical coupled welding structures must be resolved in order to successfully assemble the comb drives.

Acknowledgements

The authors thank the U. C. Berkeley Microfabrication Facility. This research was funded by a grant from the Emerging Technologies Initiative of the U. S. National Science Foundation, by an Analog Devices Career Development Professorship, and by the Berkeley Sensor & Actuator Center, an NSF/Industry/University Research Center.

REFERENCES

[1] R. L. Alley, G. J. Cuan, R. T. Howe and K. Komvopoulos, "The effect of release-etch processing on surface microstructure stiction," *Technical Digest*, IEEE Solid-State Sensor and Actuator Workshop, Hilton Head Island, SC, 21–25, June 1992.

[2] G. K. Fedder and R. T. Howe, "Thermal assembly of polysilicon microstructures," *Proceedings*, IEEE Micro Electro Mechanical Systems Workshop, Nara, Japan, January–February 1991, pp.63–68.

[3] W. Yun, R. T. Howe and P. R. Gray, "Surface micromachined, digitally force-balanced accelerometer with integrated CMOS detection circuitry," *Technical Digest*, IEEE Solid-State Sensor and Actuator Workshop, Hilton Head Island, SC, 21–25, June 1992.

[4] W. C. Tang, T.-C. H. Nguyen and R. T. Howe, "Laterally driven polysilicon resonant microstructures," *Proceedings*, IEEE Micro Electro Mechanical Systems Workshop, Salt Lake City, Utah, February, 1989.

[5] P. Krulevitch, T. D. Nguyen, G. C. Johnson, R. T. Howe, H. R. Wenk, and R. Gronsky, "LPCVD polycrystalline silicon thin films: the evolution of structure, texture and stress," *Proceedings*, Materials Research Society Fall Meeting, vol. 202, 1990.

[6] K. S. J. Pister, "Hinged polysilicon structures with integrated CMOS TFTs," *Technical Digest*, IEEE Solid-State Sensor and Actuator Workshop, Hilton Head Island, SC, 21–25, June 1992.

[7] C. H. Mastrangelo, "Thermal applications of microbridges," Ph.D. Thesis, Dept. of Electrical Engineering and Computer Sciences, University of California at Berkeley, January 1991.

[8] D. W. Greve, "The microstructure of programmed n$^+$ pn$^+$ polycrystalline silicon antifuses," *J. Appl. Phys.*, vol. 54, no. 6, 3278–3281, June 1983.

[9] A. W. Adamson, *Physical Chemistry of Surfaces*, 5th Ed., John Wiley & Sons, New York, 1990, ch. 2.

[10] R. C. Weast and M. J. Astle, ed., *CRC Handbook of Chemistry and Physics*, 62nd Ed., Chemical Rubber Publishing Co., Boca Raton, FL, 1981.

[11] Y. C. Tai and R. S. Muller, "Fracture strain of LPCVD polysilicon," *Technical Digest*, IEEE Solid-State Sensor and Actuator Workshop, Hilton Head Island, SC, 6–9, June 1988.

[12] Y. C. Tai, C. H. Mastrangelo and R. S. Muller, "Thermal conductivity of heavily doped LPCVD polycrystalline silicon films," *J. Appl. Phys.*, vol. 63, no. 5, 1442–1447, March 1988.

[13] T. Hirano, T. Furuhata, K. J. Gabriel, and H. Fujita, "Operation of sub-micron gap electrostatic comb-drive actuators," *Technical Digest*, Transducers '91, June 1991, pp.873–876.

[14] M. W. Judy, private communication.

[15] *Maxwell User's Guide*, v. 4.31, Ansoft Corporation, Pittsburgh, PA, 1991.

[16] *ABAQUS User's Manual*, v. 4.8, Hibbitt, Karlsson & Sorensen, Inc., 1989.